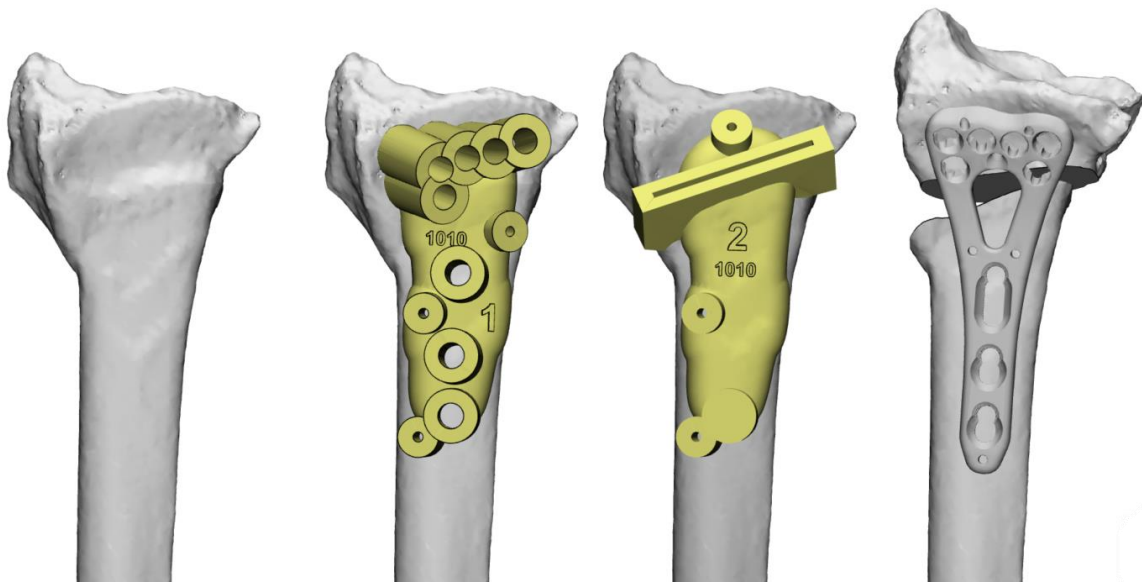


Clinical evaluation and technical optimization of patient-specific guides for corrective osteotomies of the radius

Camiel Smees - s1571796



Head
Medical Supervisor
Technological Supervisor

Guidance Counsellor
External member

Prof H.F.J.M. Koopman
A.J.H. Vochteloo, MD, PhD
R. Fluit, PhD
F. Schröder, MSc
B.J.C.C. Hessink-Sweep, MSc
J.M. Wolterink, PhD



**UNIVERSITY
OF TWENTE.**

TABLE OF CONTENTS

Table of contents

1. General introduction	5
2. The relation between the anatomic correction and range of motion following 3D guided corrective osteotomy of the radius: preliminary results.....	8
Abstract	9
Introduction.....	10
Methods	10
Patient characteristics	10
Data acquisition.....	11
Data processing	12
Analysis.....	13
Results	14
Discussion	18
3. An algorithm that creates postoperative 3D models based on a preoperative CT scan and postoperative X-ray images: preliminary results	22
Abstract	22
Introduction.....	23
Algorithm development	24
1. Data acquisition.....	24
2. Creation of the algorithm.....	25
3. *Evaluation of the algorithm.....	32
Discussion	32
4. General discussion.....	35
Bibliography.....	38
Appendix A: Pseudocode.....	42

CHAPTER 1

GENERAL INTRODUCTION

1. General introduction

Distal radius fractures are common fractures seen in hospitals with an incidence of 20-26 per 10,000 person-years. (1, 2) Depending on the severity of the fracture, treatment is either conservative (a below elbow cast after closed reduction when necessary) or surgical (K-wire fixation, external fixation or with a plate and screws). (3) One of the more common complications of distal radius fractures is a malunion with an overall rate of 17-33% with a higher rate after initial conservative treatment compared to the patients that were primarily treated surgically. (4-10) Malunion is healing of bone segments in an anatomical unfavourable orientation. This unfavourable orientation can result in pain, stiffness, loss of grip strength and early development of arthritis. (11-13)

Treatment of a malunion of the distal radius is on first hand conservative with physical therapy, splinting or rest to optimize soft-tissue adaptation. (9) If this approach does not achieve the desired result, surgical treatment is indicated; a corrective osteotomy. This means that the radius, and or ulna are sawn, the distal segment is reduced in the correct position and this is fixed with a plate and screws. The aim is to reduce the distal segment back into its anatomical orientation.

To achieve the optimal corrective osteotomy, the degree of correction is preoperatively determined using X-ray images in anteroposterior and lateral directions. Using these X-ray images, volar or dorsal angulation (Figure 1A), radial inclination (Figure 1B), ulnar variance (Figure 1C) and radial length (Figure 1D) can be measured. (8)

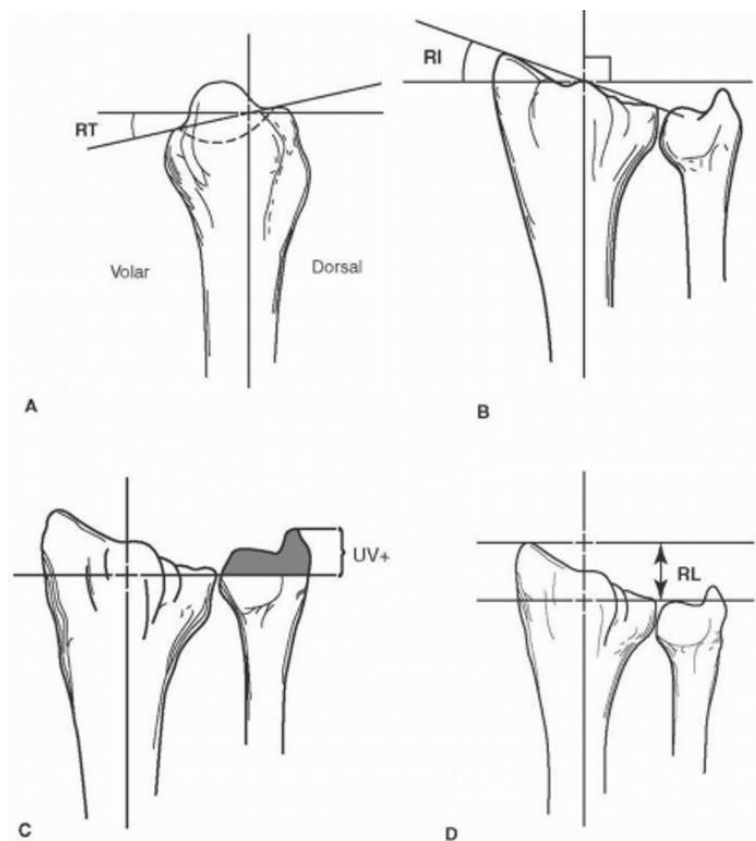


Figure 1: Radiological measurements for radius malunion. A) Volar or dorsal angulation. B) Radial inclination. C) Ulnar variance. D) Radial length. Adaptation from Graham et al. (14)

Recent studies show that X-ray images are inadequate in fully assessing a radius malunion due to the inability to detect the axial rotation, rotation of the bone in pronation or supination, Figure 3. (15) This resulted in a shift towards assessment with a CT scan to plan the optimal corrective osteotomy.

The introduction of preoperative CT scanning and its capability of precise planning of the corrective osteotomy led to the need for a technique to accurately achieve the planned correction during surgery. This was achieved through the introduction of 3D patient-specific guides (PSGs). The planning of the corrective osteotomy is used to plan the position of the plate and screws. Based on this planning, PSGs are created.

A PSG is a 3D printed tool that is designed to guide the surgeon to acquire the preoperatively planned correction. The PSG is designed to perfectly fit the surface of the patient's bone. The PSG then guides the surgeon to where holes for the plate should be drilled, Figure 2B. After drilling all the holes for the screws, the bone is sawn through the saw guide in the PSG, Figure 2C. The plate can now be fixated to the distal radius using screws in the previously drilled holes. By aligning the proximal portion of the plate to the holes in the proximal radius segment, the planned orientation of the distal radius is acquired, Figure 2D. (15)

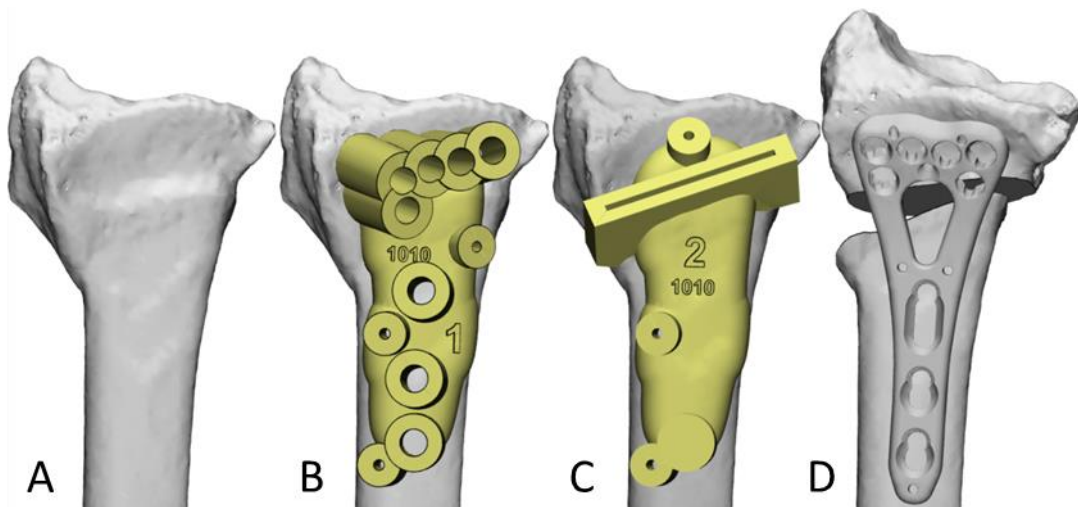


Figure 2: PSG and postoperative orientation. A) preoperative radius. B) Drill PSG. C) Saw PSG. D) postoperative radius.

After surgery, patients have check-ups at 6 weeks, 3 and 12 months; a combination of history taking, filling out questionnaires, physical examination, and X-rays. Questionnaires used are Numeric Pain Rating Scale (NPRS), Patient Rated Wrist and Hand Evaluation (PRWHE) and Patient-Specific Complaints (PSK). Physical examination consists of range of motion (ROM), see Figure 3, and grip strength measurements.

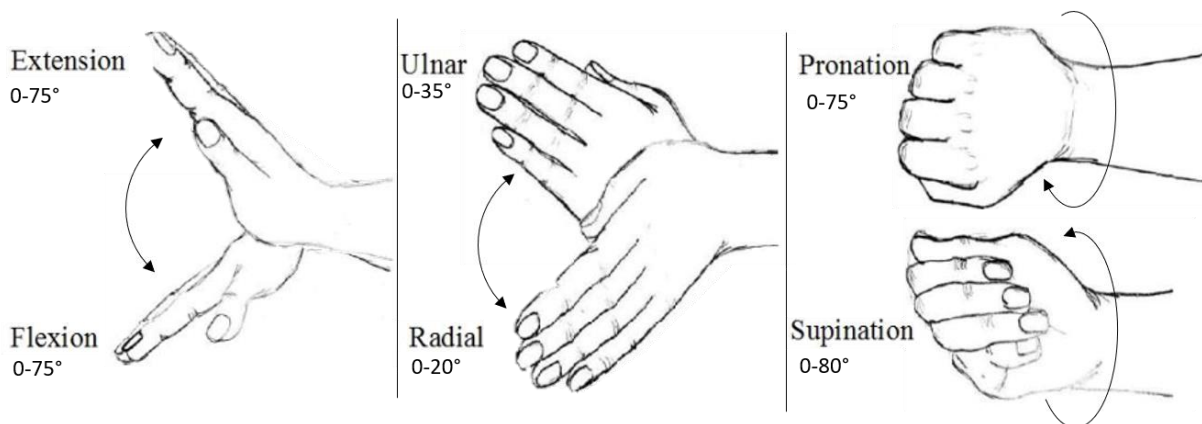


Figure 3: Range of motion measurements of the wrist. Values stated are healthy reference values. Adaptation from Adib et al. (16)

Although the use of PSGs has been widely adopted, research that objectively evaluates the benefits of PSG usage is scarce. This is mostly due to a lack of statistical power or a wide disparity of patient cases. Additionally, clinical evaluation of surgery is often based on conventional X-ray images, 2D. Since preoperative 2D images have shown to be inadequate in full assessment of the problem, it is logical that 2D-based postoperative evaluation also lacks the required information.

This thesis aims to improve the usage and evaluation of PSGs in corrective osteotomies of the radius. Therefore, firstly, the correlation between the preoperative surgical plan and the surgical result will be investigated. This will be achieved both objectively through CT-scan comparisons as well as subjectively by investigating the relation between the degree of deviation from the plan and the effect on patient related outcome measures.

Secondly, the postoperative evaluation is improved by developing an algorithm to match postoperative X-ray images to the preoperative CT scan to create a 3D representation of the postoperative radius which can be used to evaluate the postoperative situation in 3D.

CHAPTER 2

THE RELATION BETWEEN THE ANATOMIC
CORRECTION AND RANGE OF MOTION FOLLOWING
3D GUIDED CORRECTIVE OSTEOTOMY OF THE
RADIUS: PRELIMINARY RESULTS

2. The relation between the anatomic correction and range of motion following 3D guided corrective osteotomy of the radius: preliminary results

Abstract

Introduction - Malunion is the most common complication after a distal radius fracture. Surgical treatment of a radius malunion is performed through corrective osteotomy. A high degree of anatomical accuracy is required to realize the optimal postoperative result. Introduction of 3D patient specific guides (PSGs) leads to the ability to precisely plan and perform a corrective osteotomy. It is hypothesized that there is a correlation between the accuracy of anatomic correction and range of motion (ROM). Therefore, this study aimed to find this correlation.

Methods - Pre- and postoperative CT scans were acquired in 4 patients that underwent a corrective osteotomy of the radius using PSGs. Preoperative CT scans were used to obtain a 3D planning of the surgery and the PSGs. To determine the accuracy of the anatomic correction, the orientation of the radiocarpal joint on the postoperative CT scan was identified and matched with the preoperative plan. Additionally, ROM was measured pre- and postoperatively. The differences in pre- and postoperative orientation of the distal radius (i.e., the anatomic correction) were correlated to the postoperative ROM.

Results - As expected, a corrective osteotomy resulted in a change in orientation of the radiocarpal joint compared to the preoperative imaging. Overall, the position of the radiocarpal joint was corrected from a total difference preoperatively of $26.3 \pm 1.9^\circ$ with respect to the preoperative planning to $10.2 \pm 3.4^\circ$ postoperatively. In all patients, the ROM improved from $285 \pm 35^\circ$ preoperatively to $334.3 \pm 25.6^\circ$ postoperatively.

Conclusion - The preliminary results of this study showed a relation between the accuracy of anatomic correction (i.e., improved orientation of the radiocarpal joint) and improvement in ROM. No statistically significant values were obtained due to the limited number of patients.

Introduction

The most frequent complication after a distal radius fracture is a malunion, with an incidence rate of 17-33%. (4-10) The most common symptoms of a distal radius malunion are pain, stiffness, loss of grip strength, and early development of arthritis. (11-13) Treatment of a distal radius malunion is performed through a corrective osteotomy of the radius. The surgery consists of cutting the distal radius, placing the distal radius into the anatomical orientation, and fixating it using a plate and screws. Studies found a positive correlation between a high degree of accuracy of anatomical correction and a better functional outcome. (17 , 18) The need for high anatomical accuracy together with recent advancements in radiological imaging led to the introduction of CT scans in planning an osteotomy of the distal radius. CT scans have shown to more accurately assess the radius malunion. (19) The use of CT scans subsequently led to the development of 3D patient-specific guides (PSGs) for their capability of transferring CT-based planning to the operating room. These PSGs are used to guide the surgeon in performing the surgery exactly like the planning intends (20), expectedly leading to better clinical outcome.

Nowadays, the measurement of accuracy of surgery is based on a combination of radiological measurements, functional outcome, i.e. pain, strength and range of motion (ROM), and patient related outcome measures (PROMS) (10). Even though the use of PSGs is widely adopted, little evidence has been published regarding the impact of using PSGs for a corrective osteotomy on functional outcome. Thus far, most articles have solely used 2D radiographs for postoperative evaluation of the correction. (10, 13, 21) By comparing pre- and postoperative CT scans, accurate 3D measurements can be performed, thus the degree of anatomical correction can be measured more precisely. This should result in better detection of the benefits of PSG usage in radius osteotomies. We expect that the use of PSGs will result in better postoperative radiological outcomes and that this will subsequently result in better postoperative PROMS and functional results. Therefore, we aimed to find the correlation between the degree of accuracy of anatomical correction and the difference between pre- and postoperative ROM using 3D pre- and postoperative imaging.

Methods

Patient characteristics

A prospective follow-up study on 20 patients is started from December 2020 until final inclusion. The study is performed with patients with an indication to undergo a corrective osteotomy of the radius using in-house designed PSGs. CT scans are obtained of all patients both pre- and postoperatively (3 months). Additional inclusion criteria were preoperative functional measurements, PROMS, X-ray and CT, and 18 years of age or more. Exclusion criteria were age < 18 years, no reasonable understanding of the Dutch language, previous surgery on one of the wrists (both the injured and the contralateral side), need for additional procedures with the osteotomy and contraindication for CT imaging.

Inclusion occurred in the period between the operation and outpatient visit 6 weeks after surgery. Signed informed consent was obtained regarding the permission to report on their medical history, demographics, characteristics, and postoperative results, as well as to perform an additional CT scan. Ethical approval was obtained from the ethical committee of MEC-U located in Nieuwegein, code 100.

Inclusion is still ongoing past February 2021 until 20 patients are included, which was calculated in our sample size calculation. This sample size was calculated to test for Pearson correlation with an alfa of 0.05, a power of 0.8, an expected correlation R1 of 0.6 and a R0 of 0.0. These values were based on the results published by Vlachopoulos et al. (22).

Data acquisition

Of each patient, demographic information consisting of sex, age, injured side, dominance and time between fracture event and surgery were extracted from the medical history and documented.

Standard anteroposterior and lateral X-ray images were acquired preoperatively and 3 months postoperatively. Standard radiographic measurements, consisting of radial inclination, radial height, ulnar variance, and ventral-dorsal tilt, were performed on each set of X-ray images. Normal values for these radiological measurements are 19 - 25° radial inclination, 10 - 15mm radial height, -0.8 - 2.2mm ulnar variance and 6 - 16° volar tilt. (23)

CT scans were acquired preoperatively and 3 months postoperatively following a standard CT protocol for forearm scanning (24). Patients were asked to hold both arms above their head while lying in the CT scanner to minimize radiation dose.

The CT scans were loaded into Mimics (Materialise, Leuven, Belgium) in which they were converted to 3D models. This was achieved through a series of steps. First a threshold is applied to detect all dense structures in the CT scan. Second, all bone segments are selected using a built-in region growing function. The bones are visually inspected and appropriate editing is performed to delete artifacts. Finally, the bones are filled after which they are exported as 3D models.

The 3D models were then loaded into 3-Matic (Materialise, Leuven, Belgium) in which a surgical plan was made through the following steps:

1. The healthy contralateral radius is mirrored after which the mirrored radius is projected on the malunited radius.
2. Optimal proximal matching is searched for, after which the distal malalignment is assessed.
3. The plane to cut the radius is identified and verified by the surgeon performing the surgery.
4. Using the determined plane, a virtual cut is made, after which the distal radius is moved to best align with the mirrored radius.
5. A plate that will fixate the orientation during surgery is fit to the radius.
6. The holes in the plate are identified and matched to the radius as drill locations.
7. The distal radius is moved back to the preoperative situation while the drill locations attached to the distal radius move with the distal radius.
8. Based on all drill locations of both the proximal and distal segment, a guide is made that uses the surface of the 3D model to fit the bone.
9. A guide is made based on the cutting plane that also uses the surface of the 3D model.
10. A 3D model of the planned situation is made, consisting of the proximal radius and the distal radius matched to the mirrored radius.

The following measurements were performed preoperatively and 3 months postoperatively by a hand therapist:

- Range of motion (ROM) with normal values between brackets, consisting of flexion (75°), extension (75°), pronation (75°), supination (80°), radial deviation (20°) and ulnar deviation (35°), all measured in degrees. All individual values combined result in a value for total ROM (360°). (25) A total ROM of less than 300° is our definition of functional impairment.
- Grip strength, measured in kg.
- Patient-rated wrist-and hand evaluation (PRWHE), measuring pain and disability on a scale from 0-100. A lower score correlates with a better function.
- Numeric pain rating scale (NPRS), measuring minimal and maximal pain on a scale from 0-10, 0 meaning no pain and 10 the worst possible pain.

- Patient specific complaints (PSK), in which the patient addresses 3 to 5 activities in which they perceive difficulty due to the wrist. Per activity a score between 0 and 10 is given, 0 meaning no difficulty and 10 impossibility to perform the activity.

Data processing

Before the accuracy of anatomical correction could be analysed, a series of steps were performed in 3-Matic. First, the joint surface of the distal radius on the preoperative 3D model was manually identified (Figure 4A). Then, using the fit plane function in 3-Matic, a plane was fit to the identified surface (Figure 4B). These two steps were repeated for the 3D model of the planned situation and the postoperative 3D model (Figure 4C). The preoperative plane and the planned situation plane were compared to find the planned correction. (Figure 4D) The preoperative plane and the postoperative plane were compared to find the acquired correction. Finally, the planned and acquired correction were compared to find the degree of residual error.

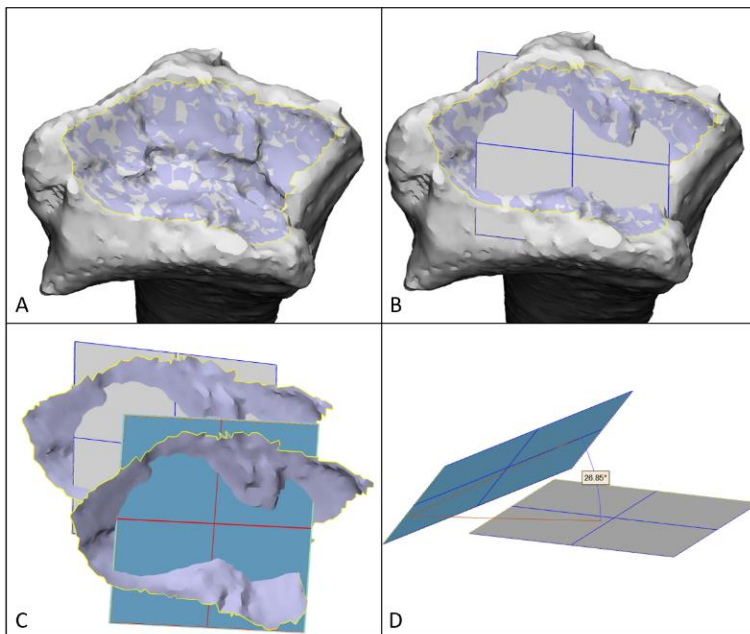


Figure 4: Creating a 3D angle. A: selecting the joint surface. B: fitting a plane to the selected area. C: performing the same steps to another CT scan (preoperative, plan, postoperative). D: determining the angle between two planes.

For standardization of results, we defined all measurements in a standard coordinate system, following the ISB guidelines. (26) We defined the X-axis as the ventral-dorsal direction, the Y-axis as the proximal-distal direction and the Z-axis as the radioulnar direction, as seen in Figure 5. For each combination of 2 planes, the difference in rotation around the X-, Y-, and Z-axis independently, as well as a combination of rotations, called the 3D angle (Figure 4), were measured, as previously described by Vlachopoulos et al. (22). Additionally, the translation in X-, Y-, and Z-direction and a combination of all translations, called the 3D translation, were measured.

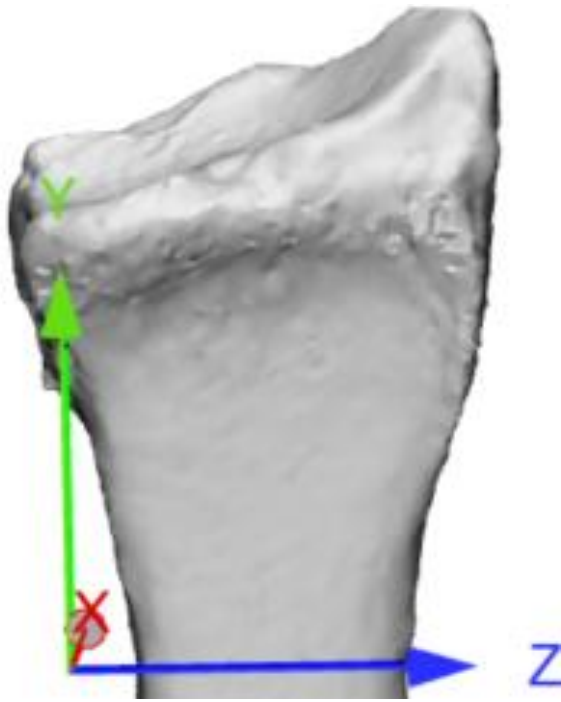


Figure 5: The definition of the coordinate system

The difference between the 3D model of the planned and achieved correction are also visually inspected using a distance map. For each point on the surface of the 3D model of the planned correction, the corresponding location on the postoperative 3D model is identified. The distance between these two corresponding points is calculated. This is repeated for all points in the 3D model. These calculated distances are converted to colours for each individual point on the 3D model. By applying the colours of all individual points on the surface of the 3D model, the whole surface of the 3D model is coloured.

Analysis

The measurements found by comparing the different 3D models were compared to the total ROM values. In this preliminary report of study data, correlations were visually inspected. Statistical testing of the correlation was performed using a Spearman correlation since normal distribution of the data could not be guaranteed due to the sample size. Surgical accuracy was defined by equation (1). This way, a value closer to 1 represents a surgical outcome that closer represents the planned correction.

$$Surgical\ accuracy = 1 - \frac{residual\ error}{planned\ correction} \quad (1)$$

Additionally, the difference in 3D angles for which the patient is functionally impaired is searched for since this value has great clinical relevance. Evaluation of additional functional measurements and PROMS was also performed visually. Radiological measurements were compared to normal values. Furthermore, the increase in functional measurements, PROMS and radiological measurements was statistically tested using a Wilcoxon signed rank test, comparing pre- and postoperative values per measurement.

Results

Table 1 summarizes the demographic data of the included patients. All patients were female, the median age was 68 years (range 63-75). In one patient, the dominant side was injured. The median time between fracture event and surgery is 10 months (range 6-14 months).

Table 1: Demographic and clinical data for each patient

Patient	Gender	Age	Dominant side	Injured side	Fracturing event to surgery (months)
1	Female	75	right	left	9
2	Female	64	right	right	14
3	Female	63	right	left	6
4	Female	71	right	left	10

Results for the planned correction and residual errors are displayed in Table 2 and Figure 6. The mean planned correction for all patients was $26.3 \pm 1.9^\circ$ and the mean residual error after surgery was $10.2 \pm 3.4^\circ$.

Table 2: Rotation and translation values for the planned correction and the residual error. Small residual error values correspond with high surgical accuracy. Abbreviations: Uln = Ulnar, Rad = Radial, Flex = Flexion, Ext = Extension, Pro = Pronation, Sup = Supination, dist = distance, Palm = Palmar Flexion, Dors = Dorsal Flexion, Prox = Proximal and Dist = Distal.

	Planned										Residual error									
	Rotation ($^\circ$)				Translation (mm)						Rotation ($^\circ$)				Translation (mm)					
	3D angle	Uln/Rad	Flex/Ext	Pro/Sup	3D dist	Uln/Rad	Palm/Dors	Prox/Dist	3D angle	Uln/Rad	Flex/Ext	Pro/Sup	3D dist	Uln/Rad	Palm/Dors	Prox/Dist				
1	26,9	38,2	27,8	9,4	10,6	6,2	7,0	5,0	10,4	14,7	11,4	2,8	5,8	3,8	2,7	3,5				
2	23,1	26,8	35,0	4,5	7,5	5,2	2,5	4,8	6,4	8,9	7,2	2,5	4,2	3,8	1,4	0,9				
3	27,0	41,5	31,0	10,2	5,1	2,6	2,7	3,5	15,6	27,3	16,5	6,0	4,3	3,9	0,9	1,8				
4	28,3	1,2	27,0	10,4	10,4	4,7	8,6	3,6	8,4	10,6	9,6	1,1	8,3	7,0	3,0	3,4				
Mean	26,3	26,9	30,2	8,6	8,4	4,7	5,2	4,2	10,2	15,4	11,2	3,1	5,7	4,6	2,0	2,4				
STD	1,9	15,8	3,1	2,4	2,3	1,3	2,7	0,7	3,4	7,2	3,4	1,8	1,7	1,4	0,9	1,1				

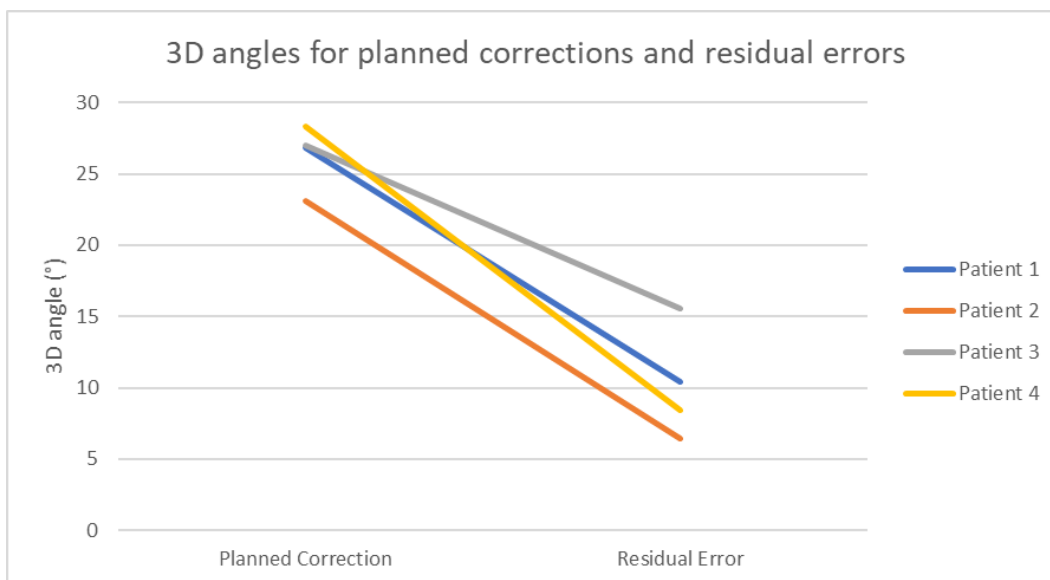


Figure 6: The 3D angle of the planned correction and the residual error. A steeper line represents a greater rotational similarity between the planned and performed orientation. A flatter line represents a smaller improvement in orientation.

In Figure 7 the distal radius in the planned orientation is displayed per patient. The colours of the surface represent the Euclidean distance between that location and its corresponding location on the postoperative 3D model. A gradient over the surface of smaller to larger distances represents a difference in rotation, while a constant colour of the entire surface represents a difference in translation.

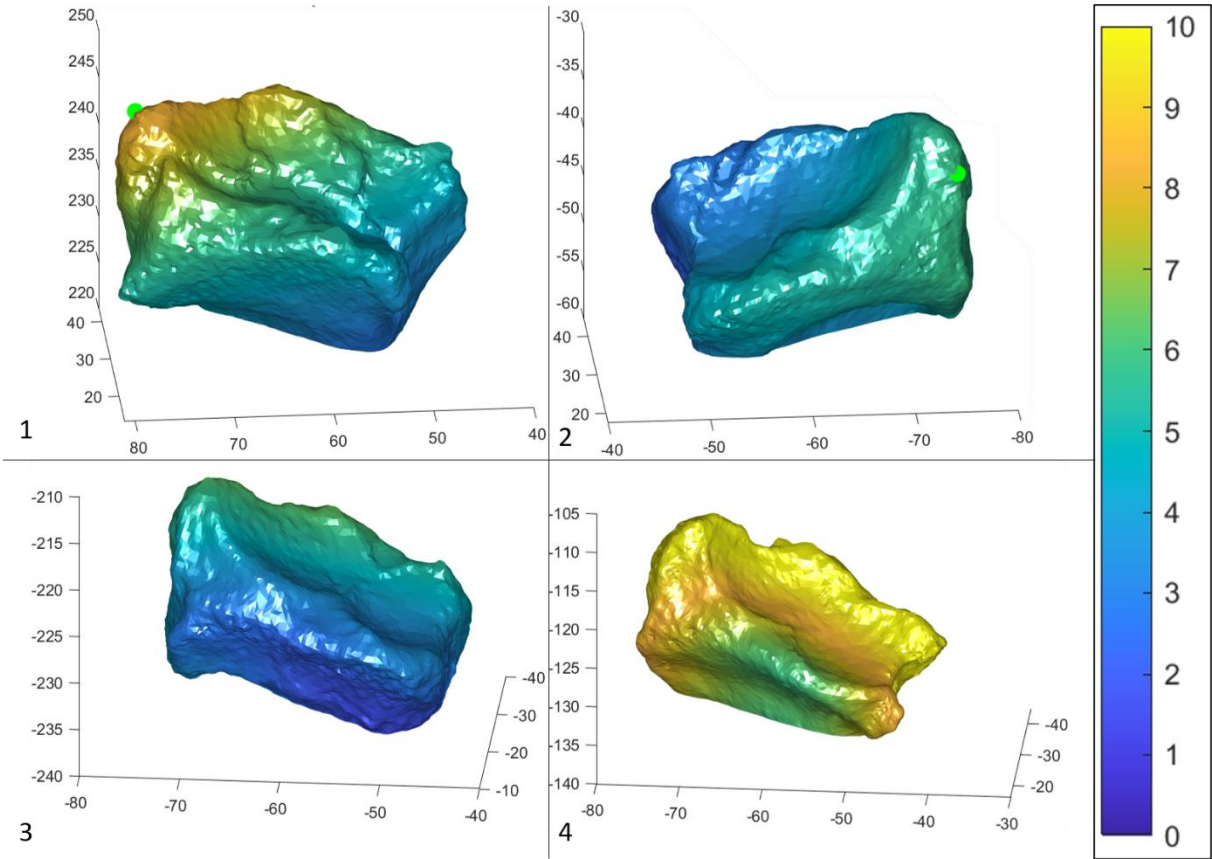


Figure 7: Distance map representing the distance per surface point between the planned and postoperative distal radius. All values are in mm and the numbers in the figure correspond with the number of the patient.

Figure 8 shows the difference in pre- and postoperative total ROM. The mean total ROM for all patients was $285 \pm 35^\circ$ preoperatively and $334 \pm 26^\circ$ postoperatively. Thus, all patients have improved total ROM after surgery with a mean increase of $50 \pm 35^\circ$ ($P=0.13$). A remarkable finding, however, is the marginal improvement in total ROM of 5° in patient 3.

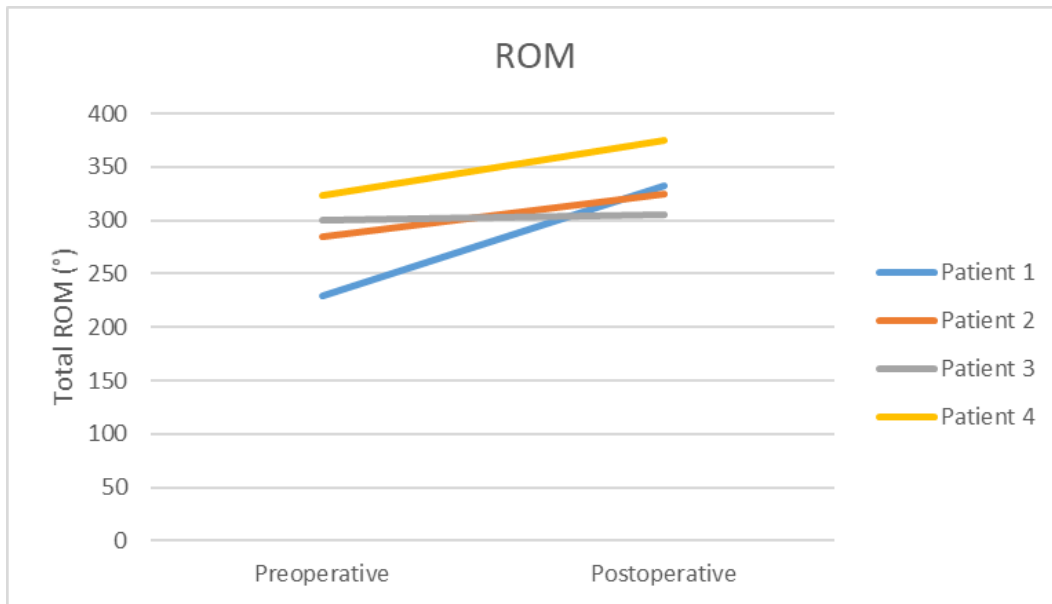


Figure 8: The total ROM value per patient pre- and postoperatively. A steep line represents a great increase in total ROM as a result of the performed surgery.

In Figure 9 the correlation between surgical accuracy and the normalized postoperative ROM is displayed. Surgical accuracy is calculated using equation (1). The postoperative ROM is normalized by dividing the postoperative ROM by the ROM of the contralateral side. Spearman correlation was not significant ($P=0.2$).

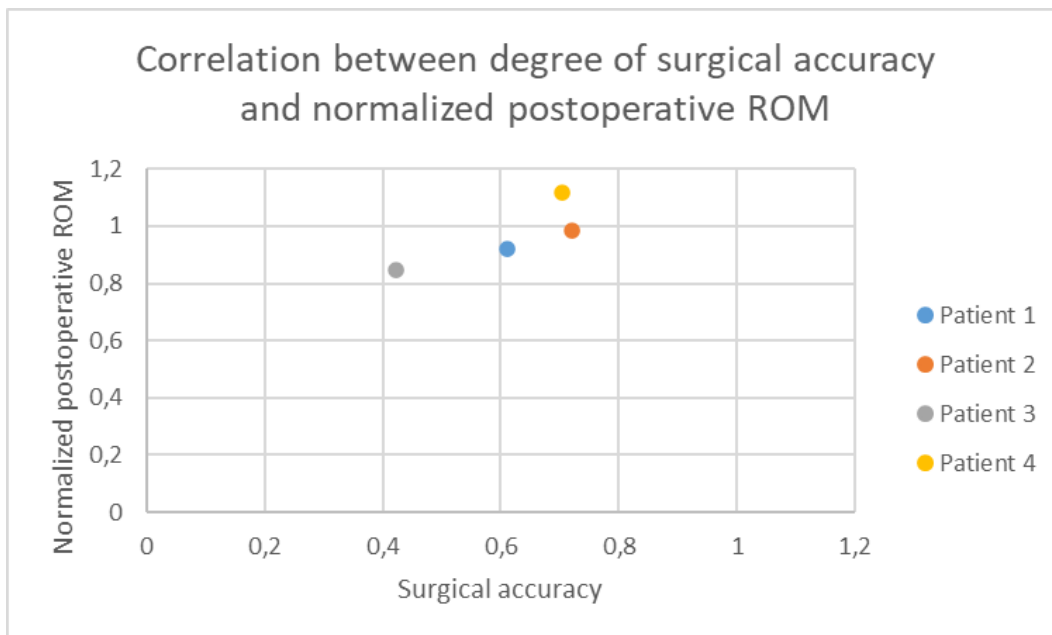


Figure 9: The correlation between surgical accuracy and normalized postoperative ROM.

When evaluating the functional measurements and PROMS, we saw a favourable progression in all measurements, as shown in Figure 10. In addition to the total ROM described earlier, all individual ROM measurements also increased ($P=0.5, 0.75, 0.5, 0.38, 0.38, 1$). The mean grip strength increased although patient 4 saw a decrease of 2 kg ($P=0.25$). All pain scores decreased ($P=0.25, 0.25$) and the overall PRWHE scores of all patients saw a favourable decrease ($P=0.13$).

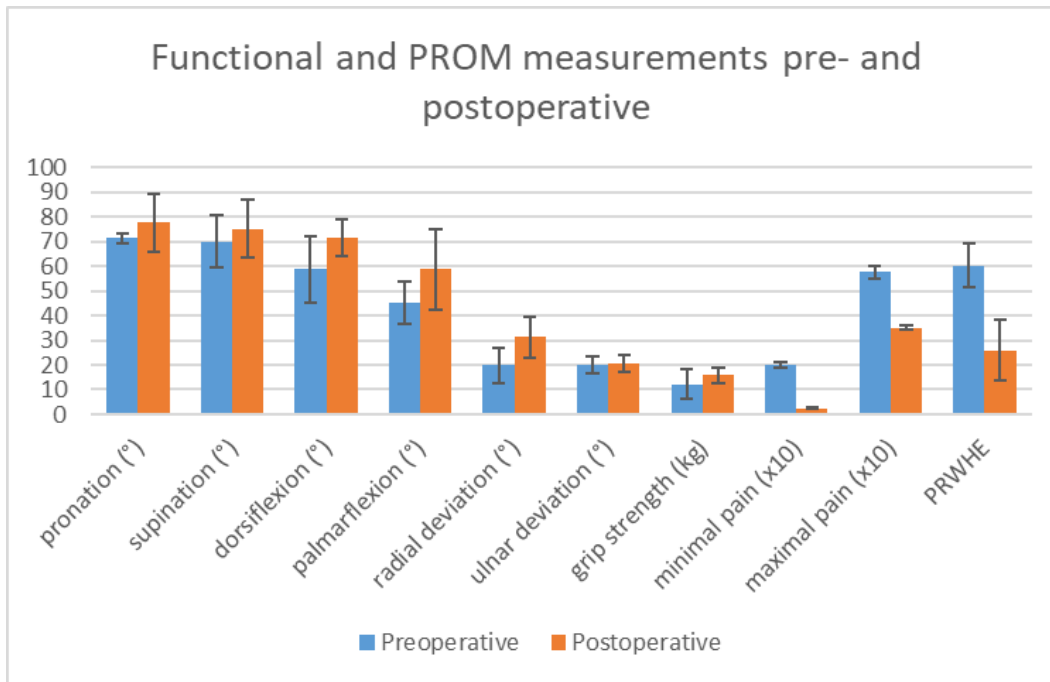


Figure 10: Functional and PROM measurements pre- and postoperative. Pain score is multiplied by 10 for visual enhancement.

When evaluating the X-ray image based radiological measurements, radial inclination, radial height, and ulnar variance was restored in patients 1, 2 and 4, while volar tilt was restored in patients 2 and 4 (Table 3).

Table 3: Radiological measurements per patient

		radial inclination (°)	radial height (mm)	ulnar variance (mm)	ventral-dorsal tilt (°)
Normal		9-25	10-15	-8-2.2	6-16
1	preoperative	13	7	3	-18
	postoperative	19	11	3	-3
2	preoperative	12	6	3	-2
	postoperative	23	12	2	11
3	preoperative	10	5	4	-19
	postoperative	15	7	4	-4
4	preoperative	18	10	2	-8
	postoperative	24	13	2	14
Mean ±	preoperative	13 ± 3,0	6,9 ± 1,8	3 ± 1	-12 ± 7,2
STD	postoperative	20 ± 3,7	10,5 ± 2,0	3 ± 1	4,4 ± 8,2

Discussion

The current study describes the correlation between the ROM and degree of anatomical correction after PSG aided corrective osteotomy of the radius. The preliminary results of the current study show an increase in ROM after surgery in all four patients with a mean increase of 50 degrees. On average, a correction of 16 degrees was achieved, which resulted in an orientation of the distal radius that better resembled the anatomical orientation of the unaffected contralateral side. The mean residual error after surgery was 10°. Based on visual inspection, a potential correlation was found between surgical accuracy and increase in postoperative ROM, as hypothesised. In one patient, a residual error of 16 degrees after a planned correction of 27° was observed. This patient also showed a marginal increase in ROM of 5 degrees and residual errors in radiological measurements. This observation further strengthens our hypothesis.

Previous studies have shown that accurate planning of a corrective osteotomy of the radius is crucial since over or under correction is associated with a decrease of ROM and other PROMS (27, 28). The residual error of $10.2 \pm 3.4^\circ$ is slightly higher than values found in other research. Vlachopoulos et al. (22) investigated the 3D angle of planned corrections in 14 patients and compared these to the residual error. They found a residual error of $5.6 \pm 4.1^\circ$ in a mean planned correction of $21.4 \pm 8.4^\circ$. The study of Stockmans et al. (29) evaluated planned and postoperative outcome of PSG aided corrective osteotomies of the radius in 3D and found residual errors of $-6 \pm 6^\circ$ in flexion-extension and $1 \pm 5^\circ$ in ulnar-radial rotation. This study did not mention 3D angles. They identified reference points normally used in X-ray image-based evaluation to measure rotational values and closest-point distance map measurements for translational errors. Other studies investigated the residual error after surgery based on X-ray images (13). Vroemen et al. (30) however demonstrated a dissimilarity between X-ray based and 3D based assessment of postoperative orientation of more than 5° making a comparison with these studies impossible. The difference in residual error in our study compared to other studies might be explained by the difference in planned correction. Our mean planned correction was $26.3 \pm 2.0^\circ$ which was about 5° larger than the surgeries performed in the stated literature. We expect that surgeries with a larger planned correction generally result in larger residual errors.

When comparing ROM values found in this study to other studies, the increase in total ROM 3 months after surgery is larger compared to studies with conventionally performed surgeries (31, 32) as can be seen in Table 4. When comparing to studies that reviewed 3D PSG aided surgeries (33, 34), lower values are found, although follow up in these studies was longer. Andreasson et al. (31) demonstrated a further increase in ROM values between 3-months follow up and 1 year follow up. Therefore, further improvement in ROM values in the current study are expected. These comparisons suggest that the use of 3D PSGs in radius correction give better postoperative ROM values compared to conventional surgery.

Table 4: pre- and postoperative total ROM values described in literature.

	Preoperative (°)	Postoperative (months after surgery; °)	Change (°)
This study	284.8 ± 34.5	334.3 ± 25.6 (3)	49.5 ± 34.7
Andreasson et al. (31) ¹	282.5	311 (3)	28.5
Malone et al. (32) ¹	244.3	286.7 (15)*	42.4
Walenkamp et al. (33) ²	239	333 (8-56)*	94
Dobbe et al. (34) ²	235	300 (6)	65
¹ = conventional surgery ² = PSG aided surgery * = only flexion-extension and pronation-supination			

When comparing the functional and PROM values to values found in literature, similar trends are found. When compared to the 3D planned group in the study of Buize et al. (13) we see a similar decrease in pain with 5.8 ± 2.6 to 3.5 ± 0.9 in our study and 6.2 ± 2.5 to 3.4 ± 2.3 in their group. In the PRWHE score, we also see a similar decrease in our population (60.3 ± 9.0 to 25.8 ± 12.3) compared to their population (58.2 ± 17.2 to 35.3 ± 28.7).

As stated in the results section, the improvement in ROM in patient 3 was noticeably smaller than the other patients. Additionally, the residual error after surgery in patient 3 was prominently higher. Investigation into medical data of this patient did not result in an explanation of the high residual error after surgery. One notable observation is that patient 3 underwent surgery using a 3D designed surgical wedge. This wedge is placed in between the proximal and distal radial segment after cutting to position the distal radius according to the surgical plan. Although this technique worked better than conventional radius correction osteotomy, we experienced that performing surgery using this technique still left margin for error. The wedge could not be fixated to the bone during alignment of the distal radius due to its size, resulting in a free-floating wedge which was manually held in place. This introduced variability in the placement of the wedge and subsequently in the positioning of the distal radius. Patient 4 and all future patients are treated using drill guides to drill holes for the fixation plate before cutting the distal radius, as described by Kunz et al. (20). We believe that this was the cause of the relative high degree of residual error.

A shortcoming of this study is the sample size, although stated in the methods section, inclusion is still ongoing. Once inclusion is finalized, the reported analysis should be reperformed to further investigate the current observations and to statistically evaluate our hypothesis. Non-parametric testing was used since normal distribution could not be guaranteed. We found that a sample size of 6 is minimum to obtain statistically significant results in two-tailed, non-parametric, exact testing with 95% confidence.

Another shortcoming of the current study is the assessment of only the complete ROM. Ideally correlations between all individual PROM values and 3D measurements should be investigated, similar to the approach of Vroemen et al. (30). Using this approach, all correlations can be identified. This way, improved insight in correlations between functional outcome and anatomical correction can be obtained. However, with only 4 patients, numbers are too low for a reliable analysis.

Contrary to most studies published, we assessed pre- and postoperative orientations of the distal radius in 3D. This enabled us to precisely measure the difference between pre- and postoperative orientations in six degrees of freedom. Additionally, many functional and PROM values were measured which can be used to investigate patient functioning and satisfaction through a combination of measurements.

We were able to visually identify a potential correlation between surgical accuracy, measured as a function of planned and performed surgery based on equation (1), and relative postoperative ROM. When inclusion is finalized, the potential correlation can be statistically tested to draw definitive conclusions.

Future research should be performed to identify more correlations between measurements of surgical accuracy and postoperative patient functioning and satisfaction. This way, we gain insight in which corrections correlate to improved postoperative results. Using these correlations, we may be able to create a prediction model for functional outcome based on preoperative radiological and functional information together with the proposed surgical correction. The model could then calculate different outcomes for the patient, based on the expected degree of surgical accuracy. This way, we can predict what degree of correction is required for optimal postoperative outcome, but also what degree of surgical accuracy must be accomplished to gain benefit of performing surgery in more complex cases.

This way we can predict what patients will benefit from surgery and what their predicted functional increase will be, while also knowing which patients should be treated conservatively based on the required surgical accuracy.

Laboratory studies have reported average residual errors of less than 1° and 1mm for simulated osteotomies that used PSGs. (35, 36) These values are considerably lower than the values found in our study and in clinical research. (13, 22, 29) In these laboratory studies, bare phantom bones are used to perform the planned osteotomy. By comparing these laboratory studies with clinical studies, the impact of the surrounding tissue on the correction can be observed. More research should be performed to identify factors that influence the degree of similarity between planned and performed PSG aided corrective osteotomies of the radius. These results could further optimise the above-mentioned prediction model.

Based on the four patients, we visually identified a correlation between surgical accuracy and increase in range of motion which strengthens our hypothesis. However, no statistical conclusions could be drawn based on the current population size. Inclusion is still ongoing, and analysis will be performed after inclusion is finalized.

CHAPTER 3

AN ALGORITHM THAT CREATES POSTOPERATIVE 3D MODELS BASED ON A PREOPERATIVE CT SCAN AND POSTOPERATIVE X-RAY IMAGES: PRELIMINARY RESULTS

3. An algorithm that creates postoperative 3D models based on a preoperative CT scan and postoperative X-ray images: preliminary results

Abstract

Introduction – Distal radius fractures are commonly seen fractures. The main complication of these fractures is malunion. Surgical treatment of malunion consists of sawing, repositioning, and fixating the distal radius. Accurate repositioning is required for optimal postoperative results. 3D planning and patient-specific guide usage was introduced to enhance accuracy of the procedure. Postoperative evaluation is still performed in 2D using X-ray images. 2D evaluation lacks information about axial deformity and is therefore suboptimal for evaluation, but routine postoperative CT examination increases radiation dose. We proposed a novel solution in which an algorithm uses the preoperative 3D model used for planning and the postoperative X-ray images to construct a postoperative 3D model which can be used to evaluate performed surgery in 3D.

Development – the 3D model of the preoperative radius was separated into a proximal and distal segment. The distal segment of the 3D model was matched based on a line along the radiocarpal joint edge. This line was manually identified in the postoperative X-ray image, while the algorithm automatically detects it in the 3D model. 2D representations of the 3D line are generated in different orientations after which the representation that best matched the 2D X-ray line is identified. Based on the corresponding orientation, the postoperative X-ray image is transformed so its orientation in 3D space matches the orientation of the distal segment of the 3D model. Within the proximal segment of the 3D model, the algorithm automatically detects the midshaft line. On the postoperative X-ray images, the midshaft line was manually identified. Matching of these lines was not yet developed. Once proximal matching is developed, the difference in orientation between the proximally matched X-ray image and the distally matched X-ray image can be identified. This difference can then be used to transform the distal section of the preoperative 3D model to find the orientation of the postoperative anatomy. After finalizing the algorithm, validation will be performed by comparing the algorithm derived 3D models to postoperative CT scan-derived 3D models.

Conclusion – the preliminary results of the current developed sections look promising. The developmental approach of the undeveloped sections is described. After successful validation, clinical implementation of the algorithm is expected to improve postoperative evaluation of corrective osteotomies of the radius.

Introduction

Distal radius fractures are common fractures with an incidence of 20-26 per 10,000 people. (1, 2) One of the serious complications of these fractures is a residual malunion, a bony union of the radius in an anatomically unfavourable orientation, happening in 17-33% of all distal radius fractures. (4-10) Due to the malunion, the forces on the radiocarpal and distal radioulnar joints are shifted, resulting in pain, stiffness, loss of grip strength, and in the long-term development of osteoarthritis. (11-13)

Surgical treatment of symptomatic radius malunion mostly consists of distal radius correction osteotomy surgery. This procedure includes sawing the malunited radius and changing the orientation of the distal radius to best restore the anatomical orientation. (9) Herein, accurate correction of the distal radius is required for optimal surgical outcome. (17 , 18) Nowadays, accurate planning of the surgery on preoperative CT scans and the use of patient-specific guides (PSGs) to translate the planning to the operating room are used to improve the surgical accuracy. (29 , 37)

Currently, the postoperative evaluation of the surgical accuracy is performed in 2D using X-ray images. (30) A postoperative evaluation in 3D using CT scans would be preferred as it is expected to result in a more in-depth assessment of the surgical outcome. However, routine postoperative CT scanning would significantly increase costs and radiation dose as compared to the current postoperative evaluation using X-ray images.

A novel solution to this problem could be the use of 3D/2D matching. In literature, the use of 3D/2D matching is described in intraoperative navigation to match intraoperative 2D X-ray images to preoperatively made 3D models. Using the intraoperative X-ray images, the 3D model is positioned to match the orientation of the X-ray images. This way, the great amount of information the 3D model provides can be combined with the low dose of X-ray images. (38) To solve the previously stated problem, the concept of 3D/2D matching could be used to combine the information of the preoperative CT scan and the postoperative X-ray images to construct a postoperative 3D model to be able to evaluate the postoperative result.

In literature, three methods of matching are described (38-41). Feature based matching uses distinct contours or points for matching and is mostly used when distinct features are easily recognizable within the images. The benefit of this type of matching is the usage of little geometric data, making this type of matching fast. (39) Intensity based matching uses the grayscale values in medical images and is mostly used to match CT scans and X-ray images. Since large amounts of data are compared, this type of matching is typically slow but more reliable than feature based matching. (40) Gradient based matching is an advanced matching type that uses 3D attenuation information to predict local maxima in X-ray images based on the orientation of the X-ray image and calculates the match between these maxima. The benefit of this type of matching is the ability to match X-ray images to MRI. (41) Since the distal radius has a distinct joint surface, feature based matching was chosen as the appropriate method of matching.

Theoretically, constructing a postoperative 3D model could be performed through the following rationale. By sawing the radius, a proximal and a distal radius segment are created, but the shape of the individual segments remains virtually the same. Since this cut is preoperatively planned and PSGs are used to translate this cut to the operating room, this cut can also be applied to the preoperative 3D model. The orientation of the distal segment relative to the proximal changes as a result of the performed surgery. This new orientation is examined using 2D postoperative X-ray images. By separately matching the proximal and distal segments of the radius in the X-ray images to the 3D model, different orientations of the 3D model segments are found. By transforming both segments separately using the corresponding orientation found in the X-ray images, new orientations of the 3D model segments are found. If the matching of the 3D model to the X-ray images is performed successfully, a 3D model of the postoperative situation should now be generated.

This research aimed to create and validate a 2D/3D registration algorithm that uses postoperative X-ray images and a preoperative CT scan to construct a postoperative 3D model. This postoperative 3D model can be used to evaluate the postoperative situation in 3D, in addition to the 2D X-ray images.

Algorithm development

Due to time constraints, the development of the algorithm was stopped prematurely. While all sections of the algorithm were thought out, not all sections were realized. All parts with an (*) represent unfinished parts of the algorithm. This is also displayed in the flowchart in Figure 12 through the dotted lines. The algorithm was developed using MATLAB (MathWorks, Natick, MA).

1. Data acquisition

Patient characteristics

Four patients who underwent an extra-articular corrective osteotomy of the distal radius at OCON centre for orthopaedic surgery in Hengelo using in-house made guides between December 2020 and February 2021 were included. All patients provided informed consent and ethical approval was obtained from the ethical committee of MEC-U located in Nieuwegein, code 100.

Radiological data

X-ray images in anteroposterior (AP), Figure 11A and 1D, and lateral direction, Figure 11B and 1E, of the pre- (Figures 1A to 1C) and postoperative (Figures 1D to 1F) situation were obtained. Both the healthy and the affected side were imaged preoperatively. Additionally, a preoperative and postoperative CT scan of the lower arms was obtained. These CT scans were made following a standard CT forearm scanning protocol (24). Both the pre- and postoperative CT scans were used to create 3D models of the radius using Mimics (Materialise, Leuven, Belgium), Figure 11C and Figure 11F.

The preoperative 3D model was used to create a preoperative surgical plan for clinical purpose using 3-Matic (Materialise, Leuven, Belgium). Based on this surgical plan, the preoperative 3D model is separated into a proximal and a distal segment, depicted respectively by the white and blue segments in Figure 11C.



Figure 11: Radiological data of the affected side from one patient. A) Preoperative anteroposterior X-ray image. B) Preoperative lateral X-ray image. C) preoperative 3D model, separated in a proximal (white) and distal (blue) segment. D) Postoperative anteroposterior X-ray image. E) Postoperative lateral X-ray image. F) postoperative 3D model.

2. Creation of the algorithm

The edge of the radiocarpal joint surface of the distal radius is a distinct 3D feature that can be identified on both the X-ray images (Figure 14) and preoperative CT scan (Figure 17). The radiocarpal joint surface does not change shape when an extra-articular osteotomy is performed and can therefore also be identified on postoperative X-ray images. The joint surface does change orientation as a result of the operation. The difference in orientation of the joint surface relative to the proximal radial segment represents the performed surgical intervention.

By identifying the joint surface in the preoperative CT scan and on the postoperative X-ray images, the distal section of the preoperative CT scan-derived 3D model can be matched to the postoperative X-ray image, resulting in the distally matched X-ray images (depicted in section D in Figure 12). By also identifying the shaft of the radius on the postoperative X-ray image and in the preoperative CT scan-derived 3D model, the proximal section of the 3D model can be matched to the postoperative X-ray image based on the radial shaft (section C in Figure 12). This gives rise to the proximally matched X-ray images. The difference in orientation between the proximally and distally matched X-ray images can be used to transform the distal segment of the 3D model into the postoperative orientation, thus creating a postoperative 3D model (depicted in section E in Figure 12). Pseudocode of the created scripts can be found in Appendix A: Pseudocode.

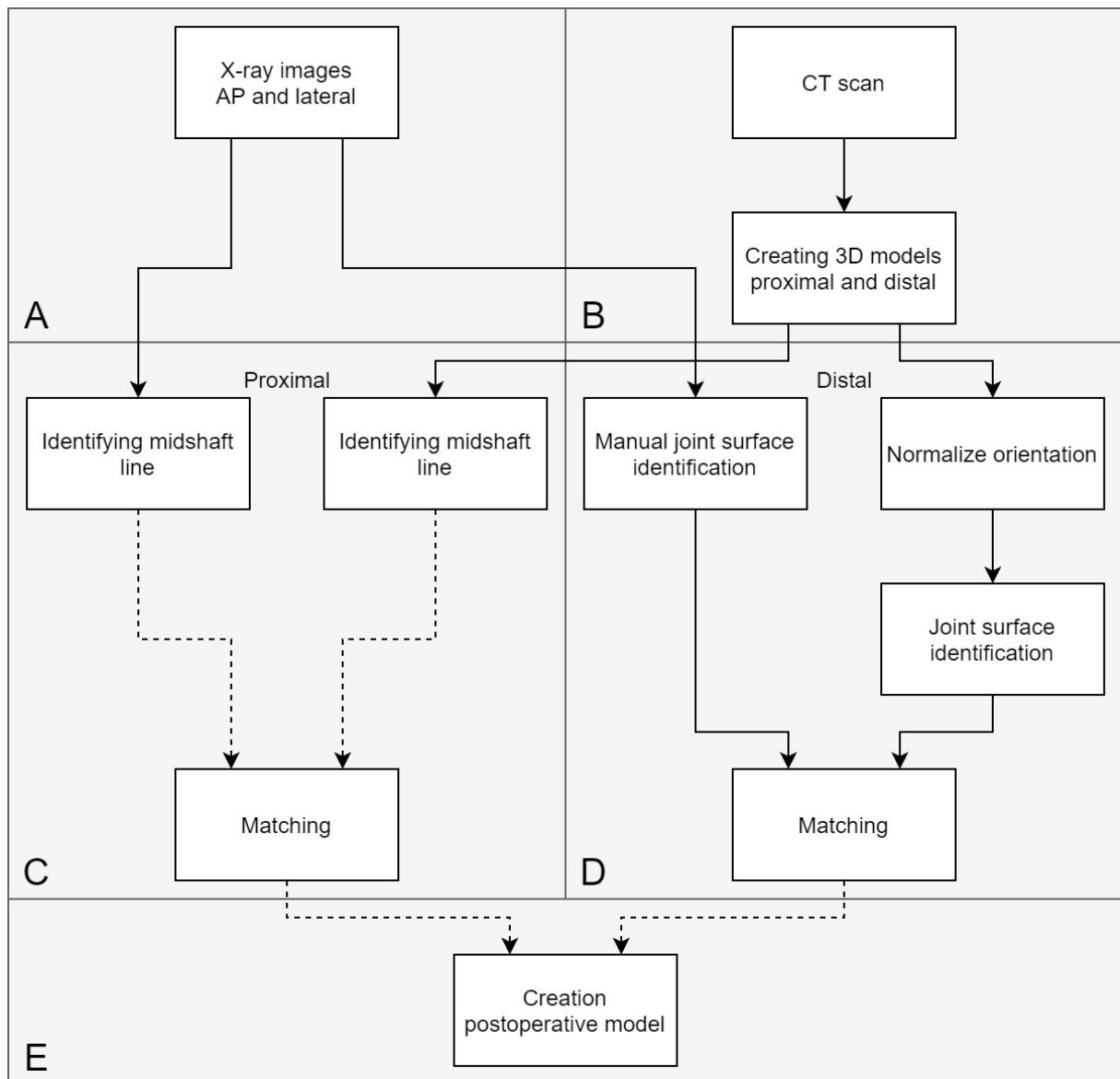


Figure 12: A flowchart describing all steps of the algorithm. The dotted lines represent unfinished portions of the algorithm.

Proximal

Midshaft line

As depicted by the steps in section C in the flowchart in Figure 12, on the postoperative AP or lateral X-ray image, the shaft of the radius is manually selected, depicted by the blue area in Figure 13A. A function that uses the edges within the image is used to assist in selecting the radial shaft. The blue area is used to fit a linear line through the area based on least-squares, as shown by the red line in Figure 13A.

On the proximal preoperative 3D model, the middle 10% and distal 10% of the model surface are selected. The means of all points that make up the surface of the model in the middle 10% and distal 10% part are calculated. This results in a mean point of the distal 10% of the proximal section and a mean point of the middle 10%. By drawing a line through these points, the midline of the proximal segment of the 3D model is generated, represented by the red line in Figure 13B.

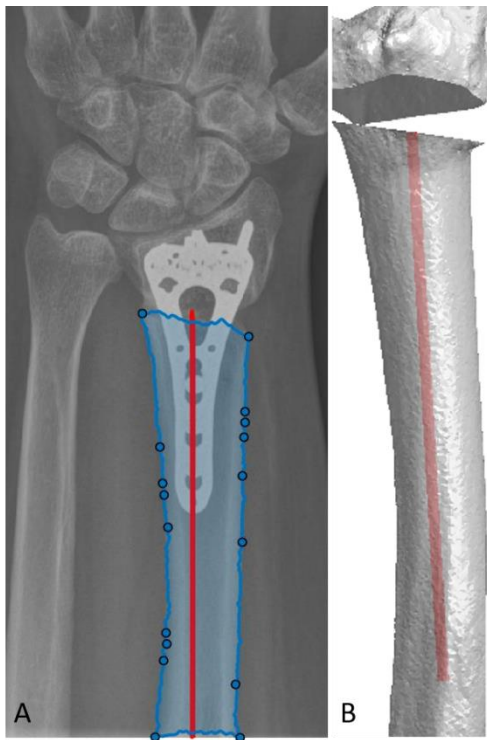


Figure 13: The midshaft line of the proximal segment. A) The midshaft line determined on the AP-X-ray image. The blue area represents the manually selected area. B) The midshaft line constructed within the 3D model.

*Matching

Perpendicular to the identified midshaft line in the X-ray images, the algorithm determines the thickness of the bone. Additionally, perpendicular to the midshaft line identified in the preoperative 3D model, the algorithm determines the thickness of the bone. Based on these measurements, the magnification factor between the X-ray image and 3D model is determined. Using this magnification factor, the length of the midshaft line in the 3D model that has to be matched to the X-ray images is determined, after which the matching of the X-ray image and 3D model is performed.

Distal

X-ray joint line

The radiocarpal joint surface is visually identified after which the line following the edge of the joint surface is manually drawn. An example is shown in Figure 14.



Figure 14: The line describing the edge of the joint surface on the postoperative X-ray image.

3D model orientation

The first step in the automatic joint line detection on the preoperative 3D model is to normalize the orientation of the 3D model. The 3D model consists of a series of triangles that together represent the surface of the model. Additionally, since the proximal and distal segments are separated by a straight cut in the postoperative situation, the proximal end of the distal segment is represented by fewer triangles than the distal end. By finding the directions of all arrows perpendicular to the triangles that make up the distal segment, the blue arrows in Figure 15, and calculating the mean of all these directions, a direction that points outwards from the joint surface is found, the yellow arrow in Figure 15. This direction is used to rotate a copy of the 3D model so that the joint surface faces towards the Z-direction. Within this new orientation, the surface point with the largest Z value, which corresponds with the radial styloid, is used to rotate the model in a standardized orientation around the Z-axis, the green point in Figure 15.

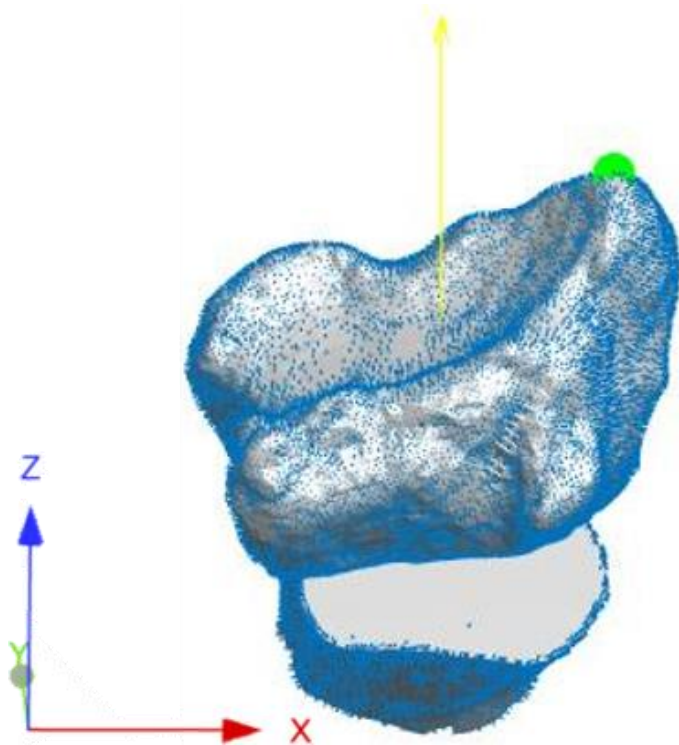


Figure 15: The orientation of the 3D model. The blue arrows represent the directions perpendicular to the individual triangles, the yellow arrow represents the mean direction of all arrows and the green dot represents the surface point with the largest Z value.

3D model points identification

All maximum locations that produce the general shape of the distal radius are identified using a Delaunay triangulation (42). A Delaunay triangulation creates a convex 3D model based on an existing model, flattening all concave areas, thus identifying all surface maxima (Figure 16A and Figure 16B). On this Delaunay triangulation, a maximum circumference per surface triangle is used to identify local islands of connected points, shown in Figure 16C with the red areas. Based on the standardized orientation, the islands corresponding with the radial styloid and the ventral and dorsal end of the distal radioulnar joint surface are identified. Of each island, the point with the maximum Z-value is identified, represented by the green points in Figure 16D. Based on these three points, the model is rotated so all three points lay in the X-Y plane.

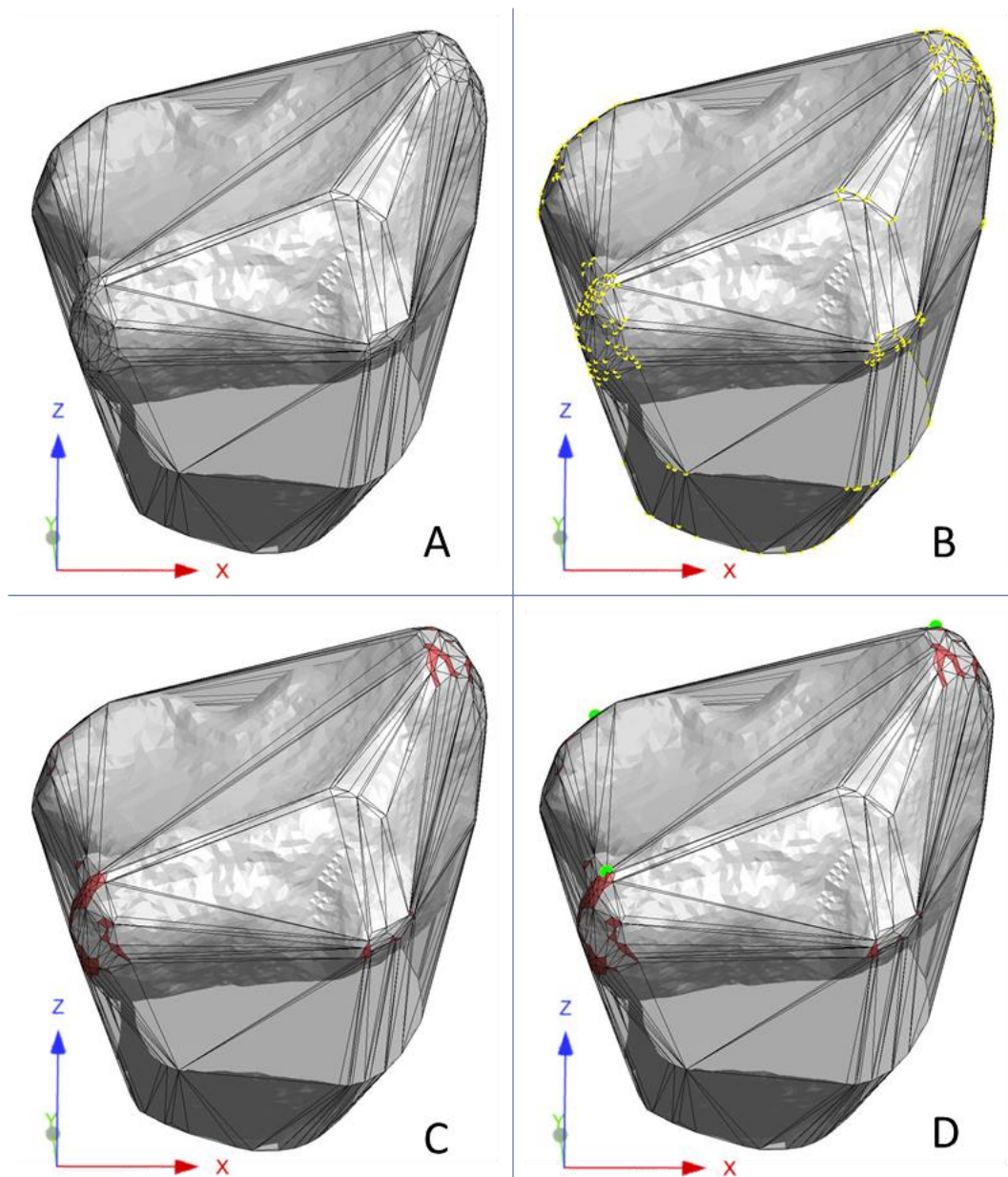


Figure 16: Identification of points. A) The model of the distal radius is shown. The Delaunay triangulation is placed over the model, shown by the black lines. B) All points where the model and the Delaunay triangulation connect are depicted by yellow points. C) In red, islands of connecting points are represented. D) In green, the selected points are shown.

3D model line calculation

Principal curvatures are calculated to identify the ridge of the radiocarpal joint surface, represented by the red areas in Figure 17. Using the restrictions of the found ridge, a path between the previously identified 3 points depicted in green is calculated. This path is found using Dijkstra's Shortest Path First algorithm (43). This algorithm assigns weights to connections between points based on user input such as height or speed, after which it finds the path between two points with the lowest total weight. The difference in Z-value between two points is used as weights for all path options. The path is generated from the previously determined points 1 to 2, 2 to 3, and 3 to 1. The weighted path is shown in blue in Figure 17. Additionally, a path is similarly generated but with equal weights, represented by the yellow line. If both lines differ too much, manual intervention is required to investigate the origin of the behaviour.

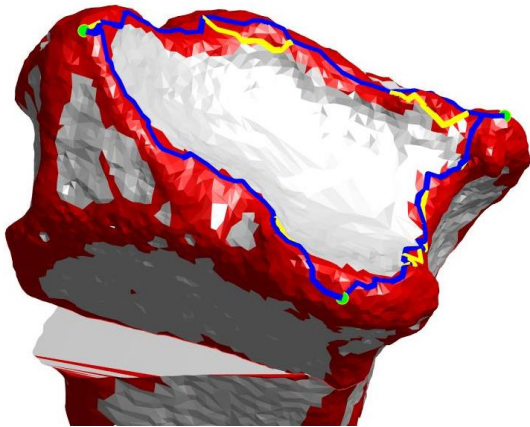


Figure 17: In red, areas with a curvature that represent edges in the model are highlighted. The 3D line that represents the edge of the radiocarpal joint line depicted in blue. In yellow, the unweighted path is represented. In green, the previously identified points are shown.

Matching

To find the best match between the 3D model derived joint surface line and the X-ray image derived line, 2D projections of the 3D line (Figure 17, blue line) in different directions are made. This is achieved by rotating the 3D line in the X-, Y-, and Z-direction or combinations of these rotations. By eliminating the X- or Y-values of the 3D line, a 2D representation is created. By using a point-to-point iterative closest point matching algorithm, all 2D representations of the 3D line are compared to the X-ray derived 2D line. Of each match, the residual error after matching is saved. The orientation of the 3D line that corresponds with the lowest residual error after matching is identified. The X-ray image is rotated by applying the inverse of the found orientation. This way, the orientation in which the X-ray image was made, relative to the distal radius is found, displayed in Figure 18.



Figure 18: The matching of the 3D model line and the X-ray image line to position the X-ray image in 3D.

**Postoperative model creation*

As depicted by segment E in the flowchart of Figure 12, after successful matching of both the proximal and distal segments on the postoperative X-ray image and the preoperative 3D model, the difference in orientation between the proximally and distally matched X-ray images can now be calculated. This difference in orientation between the proximally and distally matched X-ray images represents the difference of the proximal and distal segment in the X-ray image as a result of the performed surgery. By moving the distal segment of the preoperative 3D model by an amount equal to the difference between the X-ray images, the distal segment is placed in the position relative to the proximal section that represents the postoperative 3D model. The combination of proximal and distal segments represents the postoperative 3D model.

3. **Evaluation of the algorithm*

Due to time constraints, the algorithm could not be finalized. Therefore, it could not be used to generate 3D postoperative models and the performance of the algorithm could not be evaluated. If the algorithm would have been finalized and 3D postoperative models could have been generated, the following would have applied.

The evaluation of the algorithm would have been performed by comparing the position of the distal radius on the postoperative CT scan with the position of the distal radius based on the earlier described algorithm. First, the postoperative CT scan would have been segmented similarly to the preoperative CT scan using Mimics and a 3D model would have been created. The algorithm delivers a 3D model of the distal radius and these two models would have been loaded into 3-Matic after which they would have been moved to intersect. Registration would have been performed semiautomatically by global registration followed by manual inspection and correction. The differences between the models would have been compared by creating a distance map. Additionally, the rotational and translational differences between the distal segments would have been assessed by finding the difference in location and orientation of the distal segments by manually measuring X-, Y- and Z-displacements, a 3D angle between both orientations as well as rotation around the X-, Y- and Z-axis.

Discussion

Postoperative X-ray based evaluation of surgical accuracy is suboptimal due to the inability to assess axial rotation. (30) Postoperative CT based evaluation is expected to overcome this obstacle but introduces an increase in radiation dose and costs. The purpose of this study is to develop and validate an algorithm that creates a 3D model of the postoperative situation based on a preoperative CT scan and postoperative X-ray images. This 3D model can be used to evaluate the performed surgery in 3D. Multiple sections of the proposed algorithm have been developed and show promising results. Due to time constraints, some parts have not yet been developed although the developmental approach has been proposed. Finalization of the algorithm is required before validation can be performed.

This study successfully demonstrated first steps in the development of a novel and fully in-house made algorithm that can be used for 3D postoperative evaluation of radius correction osteotomies. Thus far, matching of the distal radius gives promising results, and the steps developed for proximal matching appear to be working properly. Additionally, for the part of the algorithm which has yet to be established, a developmental path was suggested in the Algorithm development section. Finally, a plan for verification of the complete algorithm was proposed.

After finalizing the algorithm, several thus far performed steps could be improved. Firstly, the proximal segment of the radius is currently proposed to being matched using the midshaft line in both the X-ray and 3D model. Due to the 2D nature of the midshaft line, this matching would be incapable of determining the direction in which the X-ray image was taken. This direction would therefore have to

either be assumed or be determined based on the distal matching. Both these solutions would result in uncertainty about the axial rotational difference between the proximal and the distal segment. This would result in a large margin of error in the axial rotation, defeating the purpose of this study. The proximal matching should therefore be performed differently. Since the orientation of the proximal radius is unaffected by the performed surgery and a sizeable portion of the proximal radius in the X-ray images is unaffected by the fixation plate and screws, we believe intensity-based matching is the optimal matching method.

Currently, the distal radius matching is strongly affected by the ability to reliably detect the joint surface on the X-ray image. A small error in the selection of the joint surface can result in large misalignment errors, requiring rerunning of the algorithm. This problem could be overcome by creating a movable, resizable, and rotatable 2D projection of the 3D radiocarpal joint line. This could then manually be aligned to the X-ray image to visually find the optimal match between the 3D line and the X-ray image. The orientation of the 3D line is then used to determine the transformation matrix between the X-ray image and the stand orientation of the 3D model. Using machine learning, this process could also be automated removing another manual step in the algorithm.

In future continuation of this study, after finalizing the proposed algorithm, postoperative 3D models can be generated from a preoperative CT scan and postoperative X-ray images. Before clinical implementation of the algorithm, the produced 3D models must first be verified. After finalizing inclusion of study participants, verification of the 3D models will be performed by comparing 20 postoperative CT scan-derived 3D models to the respective algorithm generated postoperative 3D models. The comparison will be performed by matching both models proximally. The difference in the distal segment is measured and displayed as differences in translation in X-, Y- and Z-direction independently, together with rotations around the X-, Y- and Z-axis. The results will be statistically tested using a non-inferiority margin that tests whether the algorithm-based 3D model is not significantly different from the postoperative CT-derived 3D model, based on the determined margin.

After successful verification of the algorithm, the technology can be implemented in regular clinical care. The use of the algorithm should enhance postoperative evaluation of corrective osteotomy surgery. The surgeon is now able to assess the performed surgery in 3D allowing him to also evaluate the axial rotation. Since the surgeon can better evaluate the surgical performance, the surgeon can better detect where to improve in future surgery. This is expected to result in lower margins of error in future surgery.

After implementation of the technique in postoperative evaluation, the intraoperative use of the technique could also be investigated. During corrective osteotomy procedures, X-ray imaging is used intraoperatively to assess the orientation of the distal radius before finishing the procedure. By using the algorithm intraoperatively, a 3D model of the intraoperative situation can be generated. By comparing this intraoperative 3D model to the preoperative surgical plan, the intraoperative orientation can better be verified. This could be beneficial in surgeries where either the PSG failed or was not used properly.

In conclusion, this study displayed preliminary results for the creation of an algorithm that can be used to create postoperative 3D models of the radius based on a preoperative 3D model of the radius and postoperative X-ray images. All steps realized thus far create desirable results, but the algorithm must be finalized before the overall performance of the algorithm can be evaluated. The final algorithm is expected to improve postoperative evaluation of radius correction osteotomy surgery by enabling 3D evaluation of the performed surgery.

CHAPTER 4

GENERAL DISCUSSION

4. General discussion

This thesis aimed to evaluate the surgical performance and optimize the postoperative evaluation of PSG aided corrective osteotomies of the distal radius. In chapter 2, we aimed to evaluate the current surgical procedure. We compared surgical accuracy, measured as a 3D angle between planned and achieved correction, with postoperative range of motion (ROM) and searched for a correlation. In chapter 3, we aimed to improve postoperative imaging-based evaluation of the performed surgery. We attempted to develop an algorithm that generates postoperative 3D models based on standard surgical planning and evaluation information, consisting of a preoperative CT scan and postoperative X-ray images.

The preliminary results found in chapter 2 suggest that there is a relation between surgical accuracy and improvement in ROM. This relation emphasises the importance of accurate reconstruction of the anatomy. This relation has been stated in previous research, where X-ray based assessment of anatomical correction was compared to postoperative ROM. (17, 18) Additionally, Vroemen et al. (30) found correlations between 3D rotational malalignment parameters and functional outcome. With statistically significant correlations between 3D rotational malalignment measurements and functional outcome, a prediction model could be generated. This model could be used to predict surgical outcome in future patients. Based on preoperative functional and radiological information, combined with the proposed correction, the model could predict a range of surgical outcomes based on the surgical accuracy of the performed surgery. This model could be used to better inform patients about the expected improvement while also identifying patients that should be treated conservatively.

In chapter 3, the development of an algorithm to generate a postoperative 3D model including the approach of the undeveloped sections is described. Although not completely finished, all developed sections work properly. Once the algorithm is finalized and validated, it will create postoperative 3D models which can be used to evaluate the performed surgery in 3D. Vroemen et al. (30) demonstrated a dissimilarity between X-ray based and 3D based assessment of postoperative orientation. We believe that 3D model based anatomical evaluation better represents the true anatomy than X-ray images. Therefore, we believe that the dissimilarity found in the study of Vroemen et al. demonstrates the achieved improvement from 3D model based anatomical evaluation compared to X-ray based anatomical evaluation.

In evaluation of surgical accuracy of corrective osteotomies of the radius, most published research uses 2D postoperative information of the performed surgery. (10, 13, 21, 30) Therefore, there is little information with regards to postoperative 3D outcome. After validation of the 3D model generating algorithm, the generated 3D models could be used in future research to provide postoperative 3D information needed for 3D evaluation of the performed surgery. This way, more 3D information about the performed correction could be generated which may lead to new clinically important insights.

Once the algorithm is validated, routine creation of postoperative 3D models could be implemented in standard postoperative care. The routine creation of postoperative 3D models and their comparison with the surgical plan gives the surgeon patient-specific information about the surgical performance. By linking the residual error of the performed surgery to the patient-specific plan, the surgeon could identify possible pitfalls in types of corrections which would improve surgical performance in future patients.

In chapter 3, we suggested that, in the future, the 3D model generating algorithm could be used in the intraoperative setting. Intraoperative X-ray images could then be used to 3D visualise the intraoperative orientation and to compare this in 3D to the surgical plan. By investigating which 3D measurements have the most impact on postoperative patient functioning, and by finding acceptable

margins in these measurements, guidelines for intraoperative use of the algorithm could be drafted. When comparing an intraoperative 3D model to the surgical plan, based on these guidelines, targeted feedback could be generated, comparable to virtual cutting guides used in craniomaxillofacial surgery (44, 45). This provides the surgeon with precise feedback about what alterations in the orientation are required to achieve the optimal operative result.

Although 3D intraoperative navigation in orthopaedic surgery is rising in popularity (46), widespread acceptance is lacking due to high costs of advance intraoperative navigation systems. (47) Although the proposed 3D intraoperative evaluation is not real time, and can therefore not replace real time 3D intraoperative navigation systems, we believe it could improve orthopaedic interventions that currently use 2D intraoperative imaging for correction assessment.

Apart from corrective osteotomies of the radius, other 3D planned orthopaedic interventions, for example trauma surgery (48), knee surgery (49) or shoulder surgery (50) could also benefit from the proposed 3D intraoperative or postoperative evaluation. The appropriate matching method should be identified for each type of surgery which is either feature based, intensity based or gradient based. Automatic detection of the important structures should be developed after which the calculation of the 3D models can be performed by the algorithm. This could lead to improvements in intra- and postoperative evaluation in a variety of orthopaedic interventions.

In conclusion, the preliminary results we found in chapter 2 seem to emphasise the importance of accurate correction of the radius when performing an osteotomy, while chapter 3 showed promising progress in building an algorithm that creates 3D models for better postoperative evaluation of surgical accuracy. The current results are promising and may lead to improvements in postoperative evaluation of the performed surgery. Furthermore, depending on the results of both studies, a variety of future studies can be started to further optimize 3D planning assisted surgery.

BIBLIOGRAPHY

Bibliography

1. Bentohami A, Bosma J, Akkersdijk GJM, van Dijkman B, Goslings JC, Schep NWL. Incidence and characteristics of distal radial fractures in an urban population in The Netherlands. *European Journal of Trauma and Emergency Surgery*. 2014;40(3):357-61.
2. Brogren E, Petranek M, Atroshi I. Incidence and characteristics of distal radius fractures in a southern Swedish region. *BMC Musculoskeletal Disorders*. 2007;8(1):48.
3. Nana AD, Joshi A, Lichtman DM. Plating of the Distal Radius. *JAAOS - Journal of the American Academy of Orthopaedic Surgeons*. 2005;13(3):159-71.
4. Athwal GS, Ellis RE, Small CF, Pichora DR. Computer-assisted distal radius osteotomy1 1No benefits in any form have been received or will be received by a commercial party related directly or indirectly to the subject of this article. *The Journal of Hand Surgery*. 2003;28(6):951-8.
5. Shin EK, Jones NF. Temporary Fixation With the Agee-Wristjack During Correctional Osteotomies for Malunions and Nonunions of the Distal Radius. *Techniques in Hand & Upper Extremity Surgery*. 2005;9(1):21-8.
6. Hirahara H, Neale PG, Lin Y-T, Cooney WP, An K-N. Kinematic and torque-related effects of dorsally angulated distal radius fractures and the distal radial ulnar joint1 1No benefits in any form have been received or will be received from a commercial party related directly or indirectly to the subject of this article. *The Journal of Hand Surgery*. 2003;28(4):614-21.
7. SHEA K, FERNANDEZ DL, JUPITER JB, MARTIN CJ. Corrective Osteotomy for Malunited, Volarly Displaced Fractures of the Distal End of the Radius*. *JBJS*. 1997;79(12):1816-26.
8. Evans BT, Jupiter JB. Best Approaches in Distal Radius Fracture Malunions. *Curr Rev Musculoskelet Med*. 2019;12(2):198-203.
9. Bushnell BD, Bynum DK. Malunion of the distal radius. *Journal of the American Academy of Orthopaedic Surgeons*. 2007;15(1):27-40.
10. Andreasson I, Kjellby-Wendt G, Fagevik-Olsén M, Aurell Y, Ullman M, Karlsson J. Long-term outcomes of corrective osteotomy for malunited fractures of the distal radius. *Journal of Plastic Surgery and Hand Surgery*. 2020;54(2):94-100.
11. Michielsen M, Van Haver A, Bertrand V, Vanhees M, Verstreken F. Corrective osteotomy of distal radius malunions using three-dimensional computer simulation and patient-specific guides to achieve anatomic reduction. *European Journal of Orthopaedic Surgery & Traumatology*. 2018;28(8):1531-5.
12. Oka K, Moritomo H, Goto A, Sugamoto K, Yoshikawa H, Murase T. Corrective Osteotomy for Malunited Intra-Articular Fracture of the Distal Radius Using a Custom-Made Surgical Guide Based on Three-Dimensional Computer Simulation: Case Report. *The Journal of Hand Surgery*. 2008;33(6):835-40.
13. Buijze GA, Leong NL, Stockmans F, Axelsson P, Moreno R, Ibsen Sörensen A, et al. Three-Dimensional Compared with Two-Dimensional Preoperative Planning of Corrective Osteotomy for Extra-Articular Distal Radial Malunion: A Multicenter Randomized Controlled Trial. *JBJS*. 2018;100(14):1191-202.
14. Graham TJ. Surgical Correction of Malunited Fractures of the Distal Radius. *JAAOS - Journal of the American Academy of Orthopaedic Surgeons*. 1997;5(5):270-81.
15. Caiti G, Dobbe JGG, Strackee SD, Strijkers GJ, Streekstra GJ. Computer-Assisted Techniques in Corrective Distal Radius Osteotomy Procedures. *IEEE Reviews in Biomedical Engineering*. 2020;13:233-47.
16. Adib M, Sahat I, Manap ZA, Ghani SAC, Hasni N, Daud N, editors. Development of the Wrist Rehabilitation Therapy (WRist-T) Device based on Automatic Control for Traumatic Brain Injury Patient2017.
17. Villar RN, Marsh D, Rushton N, Greatorex RA. Three years after Colles' fracture. A prospective review. *J Bone Joint Surg Br*. 1987;69(4):635-8.
18. McQueen M, Caspers J. Colles fracture: does the anatomical result affect the final function? *J Bone Joint Surg Br*. 1988;70(4):649-51.

19. Athlani L, Chenel A, Berton P, Detammaecker R, Dautel G. Three-Dimensional Versus Radiographic Measurements for Analyzing Extra-Articular Distal Radius Malunion. *The Journal of Hand Surgery*. 2020.
20. Kunz M, Ma B, Rudan JF, Ellis RE, Pichora DR. Image-Guided Distal Radius Osteotomy Using Patient-Specific Instrument Guides. *The Journal of Hand Surgery*. 2013;38(8):1618-24.
21. Fernandez DL. Correction of post-traumatic wrist deformity in adults by osteotomy, bone-grafting, and internal fixation. *JBJS*. 1982;64(8).
22. Vlachopoulos L, Schweizer A, Graf M, Nagy L, Frnstahl P. Three-dimensional postoperative accuracy of extra-articular forearm osteotomies using CT-scan based patient-specific surgical guides. *BMC Musculoskeletal Disorders*. 2015;16(1):336.
23. Perugia D, Guzzini M, Civitenga C, Guidi M, Domined C, Fontana D, et al. Is it really necessary to restore radial anatomic parameters after distal radius fractures? *Injury*. 2014;45:S21-S6.
24. Materialise. Forearm CT Scanning Protocol [Available from: https://www.materialise.com/system/files/resources/L-30012_CT_Protocol_Forearm.pdf].
25. Boone DC, Azen SP. Normal range of motion of joints in male subjects. *JBJS*. 1979;61(5).
26. Wu G, van der Helm FCT, Veeger HEJ, Makhous M, Van Roy P, Anglin C, et al. ISB recommendation on definitions of joint coordinate systems of various joints for the reporting of human joint motion—Part II: shoulder, elbow, wrist and hand. *Journal of Biomechanics*. 2005;38(5):981-92.
27. Schemitsch EH, Richards RR. The effect of malunion on functional outcome after plate fixation of fractures of both bones of the forearm in adults. *J Bone Joint Surg Am*. 1992;74(7):1068-78.
28. Walenkamp MMJ, de Muinck Keizer RJO, Dobbe JGG, Streekstra GJ, Goslings JC, Kloen P, et al. Computer-assisted 3D planned corrective osteotomies in eight malunited radius fractures. *Strategies in Trauma and Limb Reconstruction*. 2015;10(2):109-16.
29. Stockmans F, Dezillie M, Vanhaecke J. Accuracy of 3D Virtual Planning of Corrective Osteotomies of the Distal Radius. *J Wrist Surg*. 2013;2(4):306-14.
30. Vroemen J, Dobbe J, Strackee S, Streekstra G. Positioning Evaluation of Corrective Osteotomy for the Malunited Radius: 3-D CT Versus 2-D Radiographs. *Orthopedics*. 2013;36:e193-9.
31. Andreasson I, Kjellby-Wendt G, Fagevik Olsn M, Aurell Y, Ullman M, Karlsson J. Functional outcome after corrective osteotomy for malunion of the distal radius: a randomised, controlled, double-blind trial. *International Orthopaedics*. 2020;44(7):1353-65.
32. Malone KJ, Magnell TD, Freeman DC, Boyer MI, Placzek JD. Surgical correction of dorsally angulated distal radius malunions with fixed angle volar plating: A case series. *Journal of Hand Surgery*. 2006;31(3):366-72.
33. Walenkamp M, de Muinck Keizer R-J, Dobbe J, Streekstra G, Goslings J, Kloen P, et al. Computer-assisted 3D planned corrective osteotomies in eight malunited radius fractures. *Strategies in trauma and limb reconstruction (Online)*. 2015;10.
34. Dobbe JGG, Peymani A, Roos HAL, Beerens M, Streekstra GJ, Strackee SD. Patient-specific plate for navigation and fixation of the distal radius: a case series. *International Journal of Computer Assisted Radiology and Surgery*. 2021.
35. Ma B, Kunz M, Gammon B, Ellis RE, Pichora DR. A laboratory comparison of computer navigation and individualized guides for distal radius osteotomy. *International Journal of Computer Assisted Radiology and Surgery*. 2014;9(4):713-24.
36. Oka K, Murase T, Moritomo H, Goto A, Nakao R, Yoshikawa H, et al. Accuracy of corrective osteotomy using a custom-designed device based on a novel computer simulation system. *Journal of Orthopaedic Science*. 2011;16(1):85-92.
37. Roth KC, Walenkamp MMJ, van Geenen RCI, Reijman M, Verhaar JAN, Colaris JW. Factors determining outcome of corrective osteotomy for malunited paediatric forearm fractures: a systematic review and meta-analysis. *Journal of Hand Surgery (European Volume)*. 2017;42(8):810-6.
38. Markelj P, Tomaevi D, Likar B, Pernu F. A review of 3D/2D registration methods for image-guided interventions. *Medical Image Analysis*. 2012;16(3):642-61.

39. Xin C, Varley MR, Lik-Kwan S, Shentall GS, Kirby MC, editors. An Extension of Iterative Closest Point Algorithm for 3D-2D Registration for Pre-treatment Validation in Radiotherapy. International Conference on Medical Information Visualisation - BioMedical Visualisation (MedVis'06); 2006 5-7 July 2006.
40. Aouadi S, Sarry L. Accurate and precise 2D–3D registration based on X-ray intensity. *Computer Vision and Image Understanding*. 2008;110(1):134-51.
41. Tomazevic D, Likar B, Slivnik T, Pernus F. 3-D/2-D registration of CT and MR to X-ray images. *IEEE Transactions on Medical Imaging*. 2003;22(11):1407-16.
42. Delaunay B. Sur la sphère vide. A la mémoire de Georges Voronoï. *Bulletin de l'Académie des Sciences de l'URSS Classe des sciences mathématiques et na*. 1934;no. 6:793–800.
43. Dijkstra EW. A note on two problems in connexion with graphs. *Numerische Mathematik*. 1959;1(1):269-71.
44. Braak T, Koning S, Alphen M, Van der Heijden F, Schreuder W, Veen R, et al. A surgical navigated cutting guide for mandibular osteotomies: accuracy and reproducibility of an image-guided mandibular osteotomy. *International Journal of Computer Assisted Radiology and Surgery*. 2020;15.
45. Bernstein JM, Daly MJ, Chan H, Qiu J, Goldstein D, Muhanna N, et al. Accuracy and reproducibility of virtual cutting guides and 3D-navigation for osteotomies of the mandible and maxilla. *PLoS One*. 2017;12(3):e0173111-e.
46. Mavrogenis A, Savvidou O, Mimidis G, Papanastasiou J, Koulalis D, Demertzis N, et al. Computer-assisted Navigation in Orthopedic Surgery. *Orthopedics*. 2013;36:631-42.
47. Karkenny AJ, Mendelis JR, Geller DS, Gomez JA. The Role of Intraoperative Navigation in Orthopaedic Surgery. *JAAOS - Journal of the American Academy of Orthopaedic Surgeons*. 2019;27(19).
48. Mishra A, Verma T, Vaish A, Vaish R, Vaishya R, Maini L. Virtual preoperative planning and 3D printing are valuable for the management of complex orthopaedic trauma. *Chinese Journal of Traumatology*. 2019;22(6):350-5.
49. Fucntese SF, Meier P, Jud L, Köchli G-L, Aichmair A, Vlachopoulos L, et al. Accuracy of 3D-planned patient specific instrumentation in high tibial open wedge valgisation osteotomy. *Journal of Experimental Orthopaedics*. 2020;7(1):7.
50. Campana V, Cardona V, Vismara V, Monteleone AS, Piazza P, Messinese P, et al. 3D printing in shoulder surgery. *Orthop Rev (Pavia)*. 2020;12(Suppl 1):8681-.

APPENDIX

Appendix A: Pseudocode

3D model creation

Input: -

- Run Distal Matching Script
- Run Proximal Script

Not Finished

Distal Matching Script

Input: -

- Execute CT Distal function
- Execute Xray Distal function
- Rotate 3D path from CT Distal function in X-, Y- and Z-direction and save each orientation
- Convert each orientation to 2D by deleting either the X-, or Y-values depending on AP or lateral
- Use ICP_finite function by D. Kroon to find optimal match between X-ray points and each of the 2D representations of the 3D line, save the error
- Determine the ICP matching with the lowest error
- Determine the orientation of the 3D line corresponding with this ICP matching
- Convert the X-ray image to a 3D plane
- Use the ICP determined orientation to rotate the 3D x-ray image
- Use the mean value of the X-ray 2D line and the CT 3D line to determine the translation of the 3D X-ray image

Output: transformation matrix for the X-ray image

Proximal Script

Input: -

- Run CT proximal
- Run Xray proximal

Not Finished

CT Distal

Input: -

- GUI for manual folder selection
- Extract STL file
- Cut a duplicate STL using STLcut function
- Determine face normal
- Calculate mean of face normal
- Find vertex of maximum Z-value
- Rotate the STL so mean face normal is in Z-direction and maximum Z vertex is in X-direction, save rotation matrix
- Calculate Delaunay triangulation
- Determine circumference of each face
- Delete face if circumference is above threshold
- Determine point clouds of vertices based on residual faces
- Find maximum Z-value point per cloud

- Based on spatial location, determine 3 points
 - Point with maximum Z-value
 - Point closest to maximum X, Y and Z value in the STL
 - Point closest to minimum X, maximum Y and Z value in the STL
- Rotate the STL so the normal of the plane through these 3 points aims towards the Z-directions
- Calculate local curvature using Local Curvature
- Use local curvature to mark joint edges
- Determine weights of the marked joint edges based on Z-values
- Calculate a path between the 3 points along the marked joint edges based on Dijkstra shortest path both weighted and unweighted
 - Weighted uses determined weights
 - Unweighted uses no weights
- Find corresponding vertex locations on the initial STL
- Save locations

Output: 3D path along surface

Xray Distal

Input: -

- GUI for manual folder selection
- Read DICOM images in folder
- GUI for manual AP and lateral image selection
- GUI for region of interest selection, used to zoom to joint surface
- GUI for manual joint line selection, using drawpolyline function
- Convert drawn points based on zoomed region to location on unzoomed image

Output: X-ray images AP and Lateral, drawn point locations

CT proximal

Input: -

- GUI for manual folder selection
- Extract STL file
- Use STL cut function to keep proximal radius
- Use STL cut function to keep distal 5% of proximal radius
- Determine face normal of distal 5%
- Determine origin of all face normals
- Find mode of all face normal
- Find mean location of face normals with direction equal to the mode of all face normal
- Use STL cut function to cut proximal radius in half
- Use STL cut function to cut half radius to keep middle 5% of the proximal radius
- Find the mean location within this 5%
- Calculate line between mean of middle 5% and distal 5%

Output: line in 3D through centre of distal half of proximal radius

Xray proximal

Input: -

- GUI for manual folder selection

- Extract DICOM images
- GUI for AP and lateral image selection
- GUI for drawing line along the proximal radius, assisted using drawassisted function
- Midline calculation using fit line to scatterplot function

Output: midline through proximal radius of X-ray

STLcut

Input: triangulation, cut percentage value

- Check input
- Determine maximal value in Z-direction
- Determine minimal value in Z-direction
- Determine cut height based on cut percentage and minimum and maximum
- Find all vertices with Z-value lower than cut height
- Use Reduce Triangulation function to delete all found vertices and faces connecting these vertices

Output: triangulation

Reduce Triangulation

Input: triangulation, list of vertex numbers to remove

- Remove all marked vertices in triangulation
- Reshape faces list in triangulation from 3,n to 1,3n
- For each value in the vertex remove list
 - Find all values in faces list corresponding with the vertex
 - Find corresponding row in the faces list
 - Save all rows in separate variable
- Delete all rows of faces
- Reshape faces list
- Create triangulation with new faces and vertices lists

Output: triangulation

Local Curvature

Input: triangulation, curvature type, cut off value curvature

- Check input
- Use patchcurvature function by D. Kroon to calculate local curvature
- Based on input, determine vertices above cut off value curvature
- Reduce all values below cut off value to 0
- For each row with values equal to 0
 - Determine all rows in the faces list of the triangulation that correspond with the vertex
 - Delete the rows in the faces list
- Delete all vertices with values equal to 0

Output: a triangulation of the location with a curvature above the cut off value